

Comparative Molecular Field Analysis of A Series of Paclitaxel Analogues

Qiqing Zhu, Zongru Guo,* Niu Huang, Minmin Wang, and Fengming Chu

Department of Synthetic Medicinal Chemistry, Institute of Materia Medica, Chinese Academy of Medical Sciences, Peking Union Medical College, Beijing 100050, China

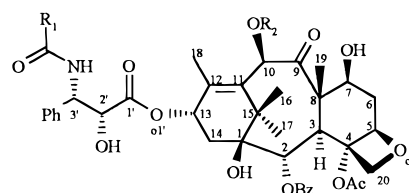
Received July 7, 1997[®]

A series of 94 paclitaxel analogues exhibiting antitumor activity by promoting the assembly of microtubules and inhibiting the disassembly process of microtubules to tubulin were investigated using the comparative molecular field analysis (CoMFA) method. These compounds belonging to 10 structural classes were randomly divided into a training set of 80 compounds and a test set of 14 compounds. Since the three-dimension structure of ligand–receptor complex is unknown, from X-ray and NMR data we rationally selected the three-dimension structure of paclitaxel in a polar solution as the active conformation and starting structure for molecule modeling, the other molecules were aligned using this molecule model as the template. The most optimal CoMFA yielded a two-components model, with significant cross-validation r^2_{cv} of 0.640 and conventional r^2 of 0.868. The predictive ability of training set model was tested on the test set of 14 compounds. The tests not only revealed the robustness of the CoMFA model but demonstrated that for our model r^2_{pred} based on the mean activity of test set compounds can accurately estimate external predictivity but r^2_{pred} based on the mean activity of training set compounds overestimated the model. The CoMFA model explained why the activity of taxoid is sensitive to the stereochemistry of the atoms at C-2' and C-3' positions and the presence of hydroxyl group at C-2' position. The other factors affecting activity were also elucidated according to standard coefficient contour maps of steric and electrostatic fields derived from the CoMFA model.

Introduction

Paclitaxel (Taxol,¹ Bristol-Myers Squibb) (**1**, Figure 1), a naturally complex diterpenoid isolated by Wall and co-worker from *Taxus brerifolia*, has been shown to have excellent antitumor activity against ovarian and breast in clinical trials.^{2–4} Phase 2 and 3 clinical trials are in progress on a wide variety of carcinomas.⁵ A semisynthetic analogue, docetaxel⁶ (**2**), is also used currently in clinical trial. Today, paclitaxel is considered by many clinical oncologists as the most promising anticancer agent. Unlike other natural “mitotic spindle poisons” such as vinca alkaloids⁷ that prevent microtubule assembly, paclitaxel has a unique mechanism of action,⁸ it blocks cancer cell division by promoting the polymerization of tubulin to microtubules and inhibits the disassembly process of microtubules to tubulin. Although both paclitaxel and docetaxel can treat various cancers, they also have some drawback such as undesired side effects and multidrug resistance.^{9–11} In addition, paclitaxel exhibits very poor water solubility. Therefore, it is essential to develop new paclitaxel analogues that have good water solubility and less or no side effects. This is the reason modification of paclitaxel has been a very hot point in drug research since it was first found to have significant antitumor activity in 1971.

Most paclitaxel analogues were semisynthetically prepared by employing the diterpene 10-deacetylbaaccatin III isolated from the plants¹² and synthetic phenylisoserine analogues.^{13,14} Extensive studies on structure–activity relationships (SAR) of paclitaxel analogues included modification on the C-13 side chain and replacement of the groups on the diterpene core. The



1 Paclitaxel: R₁=Ph, R₂=Ac

2 Docetaxel: R₁=tBuO, R₂=H

Figure 1. Structures of paclitaxel and docetaxel.

results from these explorations revealed that C-13 side chain is extremely important for outstanding antitumor activity.¹ The phenyl groups at C-3' position and C-3' *N*-acyl group can tolerate substitution of a number of bulky groups without loss of the antitumor activity.¹⁵ C-2' hydroxyl¹⁶ group and the stereochemistry 2'*R* and 3'*S* are critical for optimal activity.^{6,17} The investigation on the diterpene skeleton involving the esters at C-2, C-4, C-7, and C-10 as well as reduction of C-9 ketone^{15,18} disclosed that the substituents at C-7, C-9, and C-10 positions have less influence on the binding of the paclitaxel analogues to tubulin receptor, whereas, the oxetane ring and the groups at C-2 and C-4 are indispensable elements for the activity.

This paper gives the results of 3D-QSAR analysis for paclitaxel analogues using comparative molecular field analysis (CoMFA) introduced by Cramer et al. in 1988,¹⁹ which may establish the relationship between taxoid activities and the steric and electrostatic interaction energies calculated with a probe atom at the predefined grids. Due to the hypothesis that the most significant intermolecular interactions involved in a noncovalent binding are mainly steric and electrostatic nature, compared to classical QSAR, CoMFA directly reflects the interactions between receptor and its ligand in three

* To whom correspondence should be addressed.

© Abstract published in *Advance ACS Abstracts*, November 15, 1997.

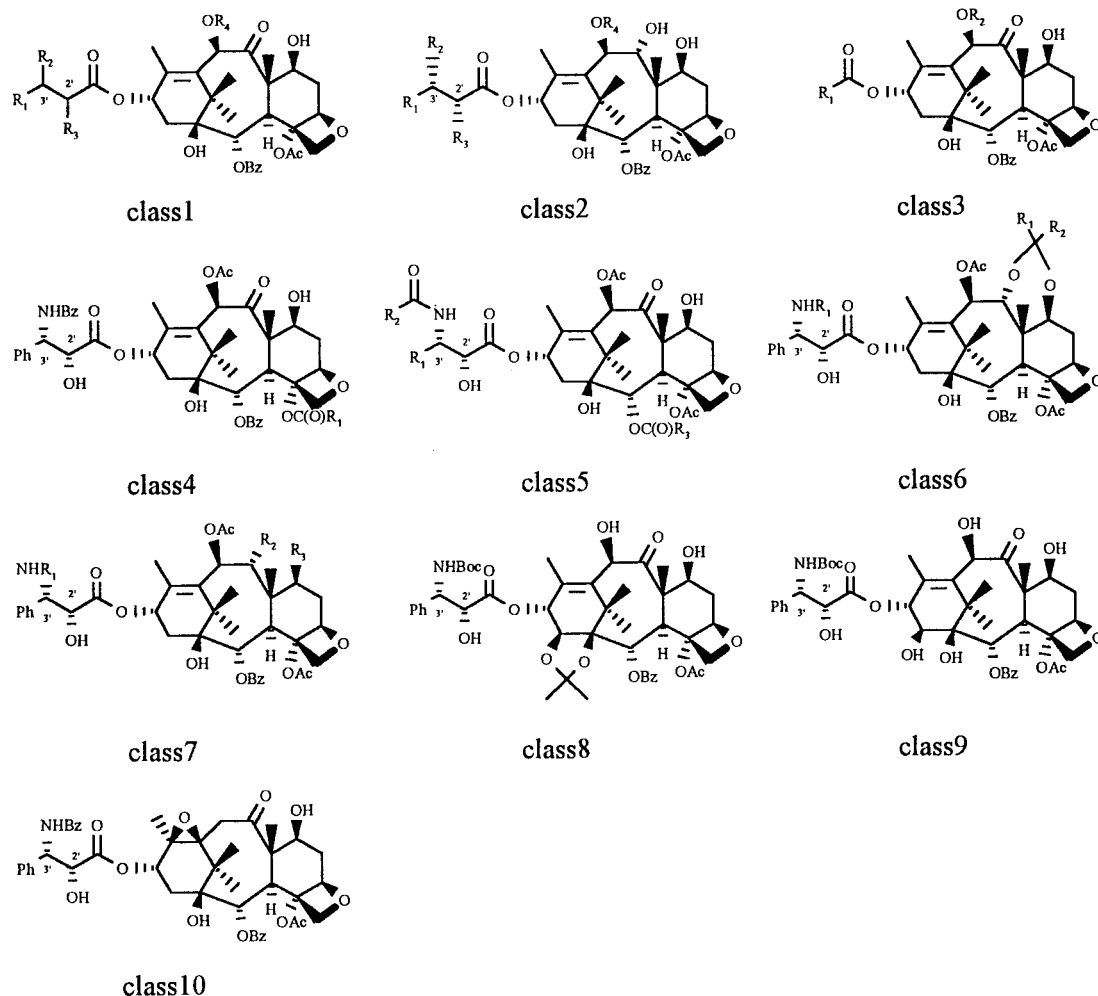


Figure 2. Structures of 10 classes of paclitaxel analogues.

dimension level. On the basis of the CoMFA model from paclitaxel analogues, we attempted to elucidate the present structure–activity relationships to provide some significant guides for the design of new paclitaxel analogues and map tubulin receptor property to a certain extent before obtaining X-ray crystallographic coordinates of a paclitaxel–tubulin complex.

Methods

Paclitaxel Analogue Selection. To develop reliable CoMFA model, 94 paclitaxel analogues with diverse structures and distinct activities were collected from the literatures.^{6,20–32} 80 analogues were randomly selected as training set, the rest as test set. According to substructural feature as shown in Figure 2, these compounds were categorized into 10 classes closely correlated with the change of substituents at all position of the paclitaxel molecule, and the corresponding substituents are listed in Table 1. The microtubule assembly activities of all compounds were expressed as the relative value of $ID_{50}(\text{analogue})/ID_{50}(\text{paclitaxel})$ (ID_{50} is the concentration of drugs leading to a 50% inhibition of the rate microtubule disassembly), and $-\log(ID_{50}(\text{analogue})/ID_{50}(\text{paclitaxel}))$ was used for the CoMFA analysis. Fourteen compounds (labeled with two asterisks in Table 1) were randomly selected to validate the predictive ability of the CoMFA model derived from the remaining 80 training set compounds.

Determination of Active Conformation. The determination of active conformation, with which ligands bind to the receptor, is crucial step for CoMFA analysis. Active conformation of flexible molecule can be obtained either from X-ray data of ligand–receptor complex or from docking active ligand into receptor or analyzing the conformation of some active molecules. Although currently the three-dimensional structure

of the paclitaxel–tubulin complex is unknown, studies on the active conformation of paclitaxel analogues were carried out by NMR spectroscopy³³ and X-ray crystallography.³⁴ These experiments have shown that all studied paclitaxel analogues in polar solution take on a conformation similar to that of the crystal structure of paclitaxel molecule B^{34d} grown from aqueous medium. Since the microtubule disassembly assay of paclitaxel was carried out in polar solution, this conformation may be most possibly related to biological activity. In the absence of 3D-structure data of the complex, it is the most reasonable to select the crystal structure of paclitaxel molecule B as the active conformation.

Molecular Modeling and Alignment Rules. All modeling work was carried out with the SYBYL6.04³⁵ software package, run on Silicon Graphics IRIS Indigo XZ-4000 workstation with default setting values except specially stated. The energy minimization of X-ray coordinates data of paclitaxel molecule B was performed with the Tripos standard molecular mechanics force field,³⁶ without inclusion of electrostatics, using the POWELL minimization technique³⁷ and distance-dependent dielectric function. The energy gradient convergence criterion was set to 0.1 kcal/mol. Partial charges were calculated with the empirical procedure of Gasteiger-Huckel. Starting from the energy-minimized structure of paclitaxel molecule B, three-dimensional structures of all the other paclitaxel analogues were built by mutating relative substituents with BUILD/EDIT-SKETCH MOLECULE option in SYBYL6.04. The unchanged atoms of paclitaxel molecule B were defined as an aggregate to hold their conformation fixed during the initial minimization. Subsequently, the aggregate was deleted and the paclitaxel analogue was fully geometrically optimized.

CoMFA, a shape-dependent technique, is highly dependent on both the conformations of the molecules considered and

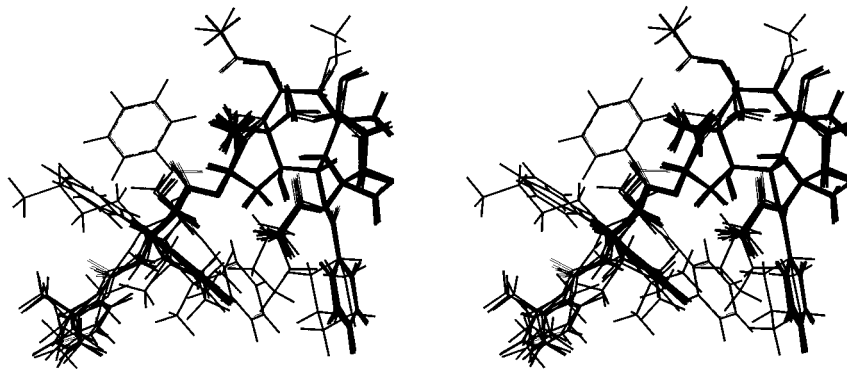


Figure 3. Stereoview of superimposition of 10 representative paclitaxel analogues.

their relative orientations.¹⁹ To define the alignment rules for the superimposition of the molecular models within a three-dimension fixed lattice, a variety of methods can be used. Here, we selected ANALYZE-FIT ATOMS (atom by atom) option for paclitaxel analogues to perform a least-squares fit between two molecules, matching the pairs of atoms. Using energy-minimized paclitaxel molecule B as a template and C1–C15, C20, O5, O1', C1'–C3' as fit atoms, the energy-minimized conformations of all remaining molecules were superimposed. Ten structurally representative molecules aligned with this strategy are shown in Figure 3.

CoMFA. The table for CoMFA analysis was built using the molecule database including the 80 paclitaxel analogues in the training set. The interaction energies were calculated at all intersections of the grid defined automatically using a sp^3 carbon atom with a charge of +1 and a distance-dependent dielectric constant. The electrostatic contributions were ignored at lattice intersections with maximal steric interactions. Different cutoff values in the range 20.0–100.0 kcal/mol, grid size (1.0 Å–3.0 Å) and field type(s) (including *both*, *steric*, and *electrostatic*), were set to investigate the effect of parameter setting values on the analysis results.

To derive regression equation from a large number of CoMFA data, partial least-squares (PLS)³⁸ was applied initially with five principal components. PLS analysis in conjunction with the cross-validation (leave-one-out method in SYBYL6.04) can give the optimal number of orthogonal components, which yield the best predictive model. The optimal number of dimensionality was chosen according to the ability to predict the data rather than to fit present data. The predictive ability of the model was expressed by the corresponding cross-validated r^2 value (r^2_{cv})¹⁹ which is defined as

$$r^2_{cv} = 1 - \text{PRESS}/\text{SD}$$

where PRESS is the sum of squared deviations between predicted and measured biological activity values for each compound in the test set and SD is the sum of the squared deviations between the measured activities of the compounds in the test set and the mean activity of the training set compounds. From the definition, a r^2_{cv} value close to 1 indicates that the model has good predictive ability. During cross-validation, we selected several column filterings (1.0–4.0 kcal/mol) to compare their effects on r^2_{cv} . Once the column filtering and the optimal number of components were determined, a final PLS analysis without cross-validation was performed. The r^2_{pred} of the 14 test set compounds was also an indicator expressing predictive ability of original model; its calculation was similar to r^2_{cv} , except that the selection of the mean activity value is subject to discussion.³⁹ Both the mean activity of test set compounds and the mean activity of the training set compounds were selected to compare their estimations for the CoMFA model.

The relationship between the biological activity and steric and electrostatic energies on the points surrounding the molecule can be shown directly in 3D space. Since CoMFA has intuitive and distinct styles, we finally used the VIEW

CoMFA procedure in SYBYL6.04 to plot CoMFA coefficient contour maps.

Results and Discussion

CoMFA Model. The statistical parameters of all PLS analyses using various options described in the method section were summarized in Table 2. The initial CoMFA of the 80 compounds in the training set using the default setting value resulted in two optimal components. This significantly predictive model was characterized by a cross-validated r^2_{cv} value of 0.643 with the SDEP (a standard error of predictions) value of 0.417. For the same data set, as noted in Table 2, the cross-validated r^2_{cv} obtained from separated steric or electrostatic field (value of 0.629, 0.637, respectively) is slightly poorer than from both steric and electrostatic fields. This indicated that either steric or electrostatic field alone cannot overall describe the 3D-QSAR of paclitaxel analogues. In general, correlation yielding a cross-validated $r^2_{cv} > 0.5$ is considered to be of predictive ability. However, the results of analysis may be partially affected by scaling of the descriptor matrixes or noise so that the model might be unstable or of chance correlation. Consequently, several individual analyses were performed to scrutinize the stability of the CoMFA model.

In the first CoMFA case, the cutoff value for both steric and electrostatic fields was set from 20.0 to 100.0 kcal/mol while the other options were the default set. The cross-validated r^2_{cv} almost remained constant as the cutoff was varied from 20.0 to 100.0 kcal/mol. The cutoff of 100.0 kcal/mol generated the best r^2_{cv} of 0.656 and increased the value of r^2_{cv} by only 0.016 (less than 5%; this is not considered as a significant improvement) from the r^2_{cv} value of 0.640 obtained with a cutoff of 20.0 kcal/mol. It has been suggested that a lower truncation (cutoff) of the probe–ligand energies which avoids unjustified large energy variance at lattice points close to the molecule in CoMFA might obtain a high-quality model;⁴⁰ a high cutoff might lead to poor correlation due to overemphasis on the interaction energies close to atoms in the molecule. On the basis of the above analysis, we selected the lower value, 20.0 kcal/mol, as the cutoff value for the next step in CoMFA.

The second case examined the effect of the grid size of the lattice box upon r^2_{cv} . Because the PLS results might be highly sensitive to the energies at discrete lattice points standing for the consecutive field energy distribution surrounding the molecule, the grid sizes of 1.0, 2.0, and 3.0 Å were separately set to calculate both steric and electrostatic interaction energies. As indi-

Table 1. Substituents and Measured Activities of All 94 Paclitaxel Analogues

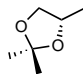
compound	R1	R2	R3	R4	act. ^a	-log(act.) ^b	ref
Class 1							
1	Ph	H	H	H	17	-1.23	6
2(2'R)	Ph	H	OH	H	4.5	-0.65	6
3(2'S)	Ph	H	OH	H	3.5	-0.54	6
4(2'R,3'S)**	Ph	OH	NHCO ₂ tBu	H	10	-1.00	6
5(2'S,3'R)	Ph	OH	NHCO ₂ tBu	H	160	-2.20	6
6(2'R,3'S)**	Ph	OH	NHCOPh	H	10	-1.00	6
7(2'S,3'R)	Ph	OH	NHCOPh	H	170	-2.23	6
8(2'R,3'S)	Ph	NHCO ₂ tBu	OH	COCH ₃	0.5	0.30	6
9(2'S,3'R)	Ph	NHCO ₂ tBu	OH	COCH ₃	30	-1.48	6
10(2'R,3'S)	Ph	OH	NHCO ₂ tBu	COCH ₃	10	-1.00	6
11(2'S,3'R)	Ph	OH	NHCO ₂ tBu	COCH ₃	108	-2.03	6
12(2'R,3'S)	Ph	NHCOPh	OH	COCH ₃	1	0.00	6
13(2'S,3'R)	Ph	NHCOPh	OH	COCH ₃	4.5	-0.65	6
14(2'R,3'S)	Ph	OH	NHCOPh	COCH ₃	10	-1.00	6
15(2'S,3'R)**	Ph	OH	NHCOPh	COCH ₃	110	-2.04	6
16(2'R,3'S)	Ph	NH ₂	OH	COCH ₃	44	-1.64	6
17(2'S,3'S)	Ph	NH ₂	OH	H	30	-1.48	6
18(2'S,3'S)	Ph	NH ₂	OH	H	30	-1.48	6
19(2'R,3'S)	Ph	NHCOPh	CO ₂ CH ₃	COCH ₃	30	-1.48	20
20(2'R,3'S)	Ph	NHCO ₂ tBu	CO ₂ CH ₃	H	10	-1.00	21
21(2'R,3'S)	Ph	NHCO ₂ tBu	OH	H	0.6	0.15	22
22(2'R,3'S)	Ph	NHCO ₂ tBu	OH	COCH ₃	0.8	0.10	22
23(2'R,3'S)	Ph	NHCO-4-CIPh	OH	COCH ₃	2.4	-0.38	22
24(2'R,3'S)	Ph	NHCO-4-CF ₃ Ph	OH	COCH ₃	6.0	-0.78	22
25(2'R,3'S)	Ph	NHCOC(CH ₃)=CHCH ₃	OH	COCH ₃	1.5	-0.18	22
26(2'R,3'S)**	Ph	NHCOCOCH ₃	OH	COCH ₃	3.5	-0.54	22
27(2'R,3'S)	Ph	NHCO-2-furan	OH	COCH ₃	0.8	0.10	22
28(2'R,3'S)	Ph	NHCO-4-MeOPh	OH	COCH ₃	0.5	0.30	22
29(2'R,3'S)	Ph	NHCO-4-MePh	OH	COCH ₃	1.1	-0.04	22
30(2'R,3'S)**	Ph	NHCOtBu	OH	COCH ₃	2.6	-0.42	22
31(2'R,3'S)	Ph	NHCOiBu	OH	COCH ₃	1.9	-0.28	22
32(2'R,3'S)	Ph	NHCOCH ₂ tBu	OH	COCH ₃	0.7	0.15	22
33(2'R,3'S)	tBu	NHCOPh	OH	H	1.8	-0.26	23
34(2'R,3'S)	tBu	NHCO ₂ tBu	OH	H	0.38	0.42	23
35(2'R,3'S)	tBu	NHCO-c-C ₃ H ₆	OH	H	0.95	0.02	23
36(2'R,3'S)	tBu	NHCO-c-C ₄ H ₈	OH	H	0.67	0.17	23
37(2'R,3'S)	tBu	NHCO-c-C ₅ H ₁₀	OH	H	1.5	-0.18	23
38(2'R,3'S)	tBu	NHCO-2-thienyl	OH	H	0.42	0.38	23
39(2'R,3'S)	tBu	NHCOCH=CH-thienyl	OH	H	2.7	-0.43	23
40(2'R,3'S)**	tBu	NHCOCH ₂ -2-thienyl	OH	H	1.9	-0.28	23
41(2'R,3'S)	tBu	NHCO-N(CH ₃)-2-pyrrole	OH	H	0.96	0.02	23
42(2'R,3'S)	4-ClPh	NHCOPh	OH	COCH ₃	2.4	-0.38	22
43(2'R,3'S)**	3,4-Cl ₂ -phenyl	NHCOPh	OH	COCH ₃	7.1	-0.85	22
44(2'R,3'S)	4-MePh	NHCOPh	OH	COCH ₃	0.8	0.10	22
45(2'R,3'S)	4-MeOPh	NHCOPh	OH	COCH ₃	0.5	0.30	22
46(2'R,3'S)	2-furyl	NHCOPh	OH	COCH ₃	0.9	0.05	22
47(2'R,3'S)	4-0HPh	NHCOPh	OH	COCH ₃	0.8	0.10	22
48(2'R,3'S)	2-pyridyl	NHCOPh	OH	COCH ₃	0.7	0.15	22
49(2'R,3'S)	naphthyl	NHCOPh	OH	COCH ₃	7.1	-0.85	22
50(2'R,3'S)	iPrCH ₂	NHCO ₂ tBu	OH	H	0.78	0.16	24
51(2'R,3'S)	tBuCH ₂	NHCO ₂ tBu	OH	H	1.45	-0.16	24
52(2'R,3'S)**	PhCH=CH	NHCO ₂ tBu	OH	H	1.45	-0.16	24
53(2'R,3'S)	(CH ₃) ₂ =CH	NHCO ₂ tBu	OH	H	0.64	0.19	24
Class 2							
54		NHCO ₂ tBu	OH	COCH ₃	7.91	-0.90	25
55	CH ₂ (OH)C*H(OH)	NHCO ₂ tBu	OH	COCH ₃	2.71	-0.43	25
56	MeOCH ₂	NHCOPh	OH	COCH ₃	3.14	-0.50	25
57	PhOCH ₂	NHCOPh	OH	COCH ₃	5.81	-0.76	25
58	CH ₃	NHCO ₂ tBu	OH	COCH ₃	1.08	-0.03	25
59	CH ₃ CH ₂	NHCO ₂ tBu	OH	COCH ₃	0.61	0.21	25
60	(3'R)-butyl	NHCO ₂ tBu	OH	COCH ₃	9.74	-1.00	25
61	c-C ₆ H ₁₁	NHCO ₂ tBu	OH	COCH ₃	0.57	0.24	25
62	Ph	NHCO ₂ tBu	OH	COCH ₃	0.87	0.06	25
63	Ph	NHCOPh	OH	COCH ₃	0.86	0.07	25
64	Ph	NHCOCH ₃	OH	COCH ₃	3.17	-0.50	26
65**	Ph	NHCONHtBu	OH	COCH ₃	1.06	-0.03	26
66	Ph	NHCO ₂ iPro	OH	COCH ₃	0.75	0.13	26
67	Ph	NHCO ₂ C ₂ H ₅	OH	COCH ₃	0.82	0.09	26
Class 3							
68**	PhCH=CH	H			23	-1.36	6
69	CH ₃ CH=CH	COCH ₃			100	-2.00	6
70**	PhCH(OH)CH(OH)	H			3	-0.48	6
71	CH ₃ CH(OH)CH(OH)	COCH ₃			60	-1.78	6

Table 1 (Continued)

compound	R1	R2	R3	R4	act. ^a	-log(act.) ^b	ref
Class 4							
72	Cl ₃ C				0.7	0.15	27
73	CH ₃ CH ₂				1.3	-0.11	27
74	CH ₂ =CH				0.6	0.22	27
75	CH ₃ CH ₂ CH ₂				0.6	0.22	27
76	c-C ₃ H ₅				0.48	0.32	27
77	CH ₃ (CH ₂) ₃				0.7	0.16	27
78**	c-C ₄ H ₇				0.9	0.05	27
79	MeO				0.7	0.16	27
80	EtO				0.56	0.25	27
Class 5							
81**	Ph	Ph	c-C ₆ H ₁₁		1.7	-0.23	28
82	Ph	OtBu	c-C ₆ H ₁₁		0.67	0.17	29
83	c-C ₆ H ₁₁	Ph	Ph		0.29	0.54	29
84	c-C ₆ H ₁₁	c-C ₆ H ₁₁	c-C ₆ H ₁₁		0.47	0.33	29
Class 6							
85	COPh	CH ₃	CH ₃		0.76	0.12	30
86	COPh	=S	=S		2.78	-0.44	30
Class 7							
87	COPh	CO ₂ CH ₃	CO ₂ CH ₃		0.91	0.04	30
88**	COPh	OH	MeO		0.92	0.04	30
89	CO ₂ tBu	OH	MeO		1.74	-0.24	30
90	COPh	MeO	OH		0.35	0.50	30
91	CO ₂ tBu	MeO	OH		0.51	0.29	30
Class 8							
92					3	-0.48	31
Class 9							
93					0.8	0.1	31
Class 10							
94					0.66	0.18	32

*S; **testing set analogues. ^a Measured activities were expressed as ID₅₀(analogue)/ID₅₀(paclitaxel), ID₅₀ is the concentration of drug leading 50% inhibition of the rate microtubule disassembly. ^b The activities used for CoMFA were expressed as the form of -log(ID₅₀(analogue)/ID₅₀(paclitaxel)).

Table 2. Statistical Parameters of All CoMFA Analyses

analysis	fields	cutoff (kcal/mol)	grid size (Å)	col filter (kcal/mol)	no. of compd	r ² _{cv} (r ²) ^a	SDEP ^b (s) ^c
01 ^d	both	30.0	2.0	2.0	2	0.643	0.417
02	steric	30.0	2.0	2.0	1	0.629	0.423
03	electr	30.0	2.0	2.0	2	0.637	0.421
04 ^e	both	20.0	2.0	2.0	2	0.640 (0.868)	0.419 (0.259)
05	both	40.0	2.0	2.0	2	0.637	0.421
06	both	50.0	2.0	2.0	2	0.642	0.418
07	both	60.0	2.0	2.0	2	0.647	0.415
08	both	70.0	2.0	2.0	2	0.655	0.411
09	both	80.0	2.0	2.0	2	0.654	0.411
10	both	90.0	2.0	2.0	2	0.656	0.410
11	both	100.0	2.0	2.0	2	0.656	0.410
12	both	20.0	1.0	2.0	2	0.650	0.414
13	both	20.0	3.0	2.0	2	0.622	0.430
14	both	20.0	2.0	1.0	2	0.641	0.419
15	both	20.0	2.0	3.0	2	0.633	0.423
16	both	20.0	2.0	4.0	2	0.611	0.436

^a Conventional r² determined with the optimum number of components. ^b Standard error of prediction. ^c Standard error of estimate. ^d Default setting value. ^e The final model, F = 96.90, steric = 70.9%, electrostatic = 29.1%.

cated in Table 2, the analysis using grid size 1.0 Å generated the best r²_{cv} value (0.650) but was an improvement of only 0.01 logarithm units from the value of 0.640 obtained with 2.0 Å and required much more computation time. Hence, all later CoMFA would select the most optimal grid size as 2.0 Å.

Leave-one-out calculation is usually performed with column filtering (minimum σ) to exclude the interaction energies that provide little or no variance for PLS analyses and improve the signal-to-noise ratio so as to obtain a better model. A higher column filtering value may reduce the lattice points so that the model does not contain enough information or accurately reflect relationships. During the column filtering, the value was increased from 1.0 to 4.0 kcal/mol with steps of 1.0

kcal/mol. We observed that the default value of 2.0 kcal/mol presented nearly the best r²_{cv} (0.640). To rationally consider the contribution of interaction energy to the activity, we selected a column filtering of 2.0 kcal/mol for the final CoMFA analysis although the other option produced an approximately equal r²_{cv}.

According to above optimal results, the final cross-validated experiment for the 80 compounds used the following setting values: 20.0 kcal/mol field energy cutoff for both steric and electrostatic fields, 2.0 Å grid size, 2.0 kcal/mol column filtering, and the remaining default setting values. The number of optimal components amounted to 2. A higher cross-validated r²_{cv} value of 0.640 with SDEP value of 0.419 indicated that the model had better predictive ability. The plot of pre-

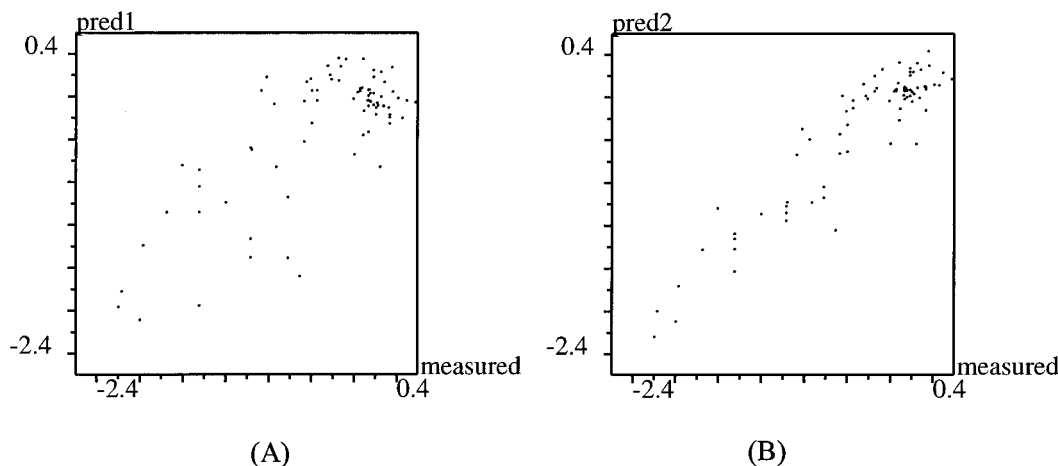


Figure 4. Plots of predicted vs measured activities of training set compounds: (A) from cross-validated model, (B) from non-cross-validated model.

Table 3. Predictive Results of All 14 Test Set Compounds

compound	measured activity	predicted activity	residual
04	-1.00	-1.27	-0.27
06	-1.00	-1.27	-0.27
15	-2.04	-2.23	-0.19
26	-0.54	-0.23	0.31
30	-0.41	0.02	0.39
40	-0.28	0.04	0.32
43	-0.85	-0.13	0.72
52	-0.16	0.05	0.21
65	-0.03	0.01	0.04
68	-1.36	-1.18	0.18
70	-0.48	-1.04	-0.56
78	0.04	0.02	0.02
81	-0.23	-0.01	0.22
88	0.05	-0.06	-0.11

dicted versus measured activity of the 80 compounds is shown in Figure 4A. The corresponding model with no cross-validation and two optimal principal components had a conventional r^2 value of 0.868 with an s (standard error of estimate) value of 0.259 and an F -test value of 96.90. The CoMFA model fits the present data well, as shown in Figure 4B. The steric and electrostatic contribution to the QSAR equation is 70.9% and 29.1%, respectively, which indicated that the steric field has more contribution in determining activity than the electrostatic field. The following approach would evaluate the predictive ability of the model with non-cross-validation.

Predictive Ability of the Model. To evaluate the validity of the CoMFA model derived from training set, the test set of 14 compounds were predicted. As shown in Table 3, the activities of these compounds were predicted within 0.716 log units of their measured activities with an average absolute error of 0.270 log units. These statistical parameters initially indicated that the CoMFA model had good predictive ability to the test compounds. The predictive results were plotted in Figure 5. Besides r^2_{cv} , external test r^2_{pred} is also an appreciable indicator validating the predictive ability of the CoMFA from training set. As mentioned earlier, we can obtain a different r^2_{pred} if selecting different mean activity: r^2_{TR} obtained by selecting the mean activity of training set compounds, r^2_{TE} obtained by selecting the mean activity of test set compounds.

After studying the 3D-QSAR of a series of steroid aromatase inhibitors,⁴¹ Oprea and co-workers observed that the training-set-based predictive r^2_{TR} (more than

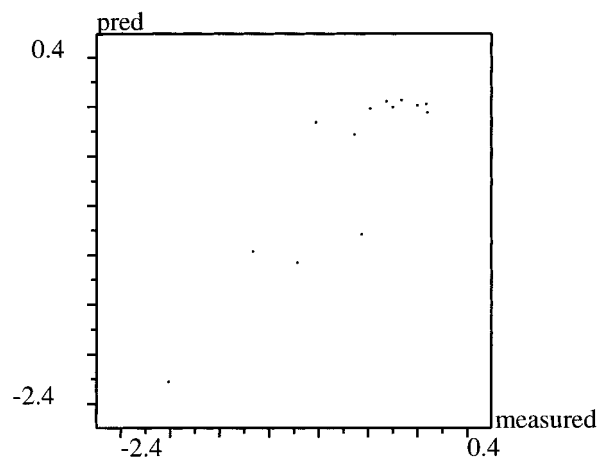


Figure 5. Plot of predicted vs measured activities of test set compounds.

0.80) led to overestimating the predictive ability of original model. On the contrary, the test-set-based predictive r^2_{TS} was highly consistent with the cross-validated r^2_{cv} . Although r^2_{TR} is used in many CoMFA literatures, it was recommended that the r^2_{TR} should be avoided, or used only in conjunction with the mean-activity-independent index such as PRESS, SDEP, and MAEP (mean absolute error of prediction). Our r^2_{TE} of 0.682, slightly more than the r^2_{cv} value of 0.640, showed it had approximate ability in describing the same model. However, the great difference (0.1 log units) between r^2_{TR} of 0.740 and r^2_{cv} of 0.640 indicated that r^2_{TR} would overestimate the model. Results from our analysis were in agreement with Oprea's conclusion: r^2_{pred} value obtained from the mean activity of the test set compounds is more accurate for evaluation of predictive ability than the r^2_{pred} value obtained from the mean activity of the training set compounds.

Coefficient Contour Map. The CoMFA steric and electrostatic fields from the final non-cross-validated analysis were plotted as three-dimension colored contour maps in Figures 6 and 7. The field energies at each lattice point were calculated as the scalar results of the coefficient and the standard deviation associated with a particular column of the data table ($stdev \cdot coeff$), always plotted as the percentage of contribution to the CoMFA equation. From a statistical perspective of the final CoMFA model, the steric field has more contribution to predicting activity than the electrostatic field does

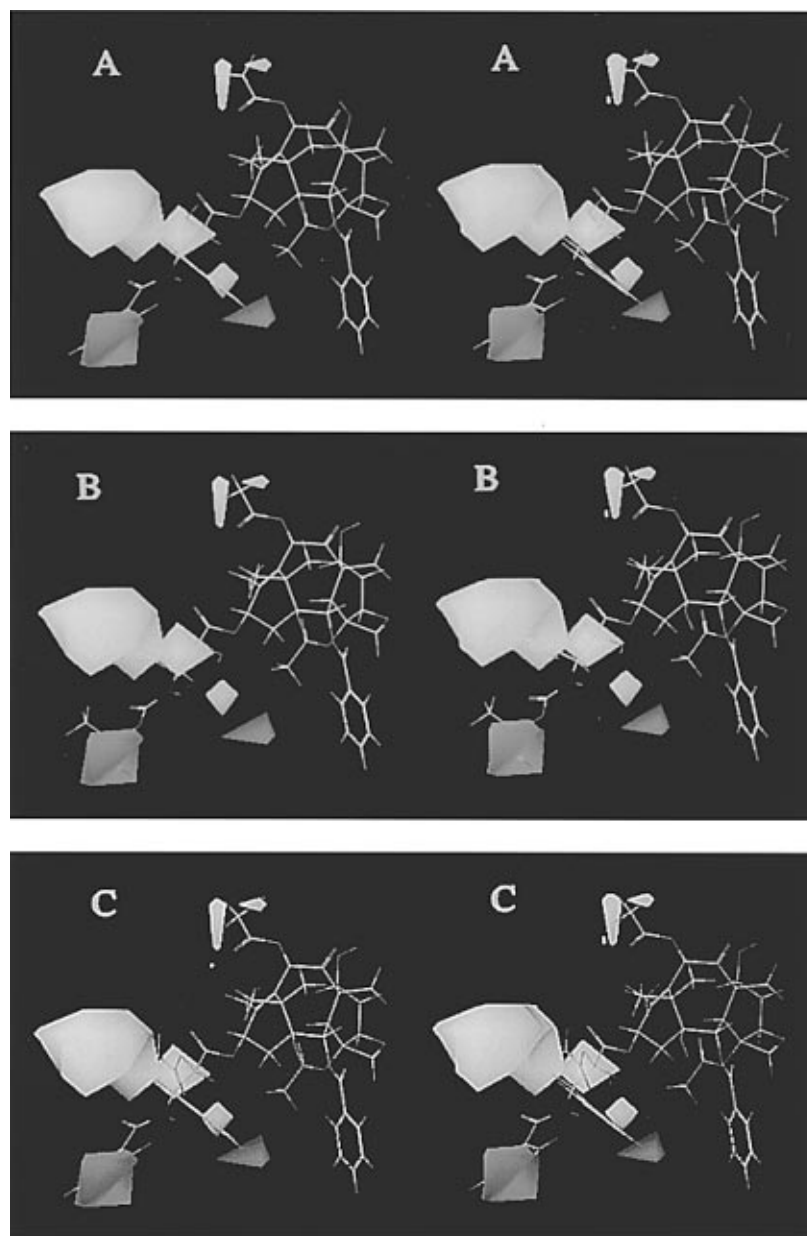


Figure 6. Stereoview of the CoMFA steric sd^*coeff contour plot from the PLS analysis based 80 training set compounds. Sterically favored areas (contribution level of 80%) are represented by green polyhedra. Sterically disfavored areas (contribution level of 20%) are represented by yellow polyhedra. Active compound **12** ((2'*R*,3'*S*)-paclitaxel), less active compound **9** ((2'*S*,3'*R*)-10-acetoxycetaxel) and less active compound **19** ((2'*R*,3'*S*)-2'-acetoxypaclitaxel) were embedded in A, B, C, respectively.

(70.9% and 29.1%, respectively). In Figure 6, green contours represent regions where bulky groups are favorable (80% contribution) to the activity, and yellow contours represent region where bulky groups are unfavorable (20% contribution). In Figure 7, the red (80% contribution) and the blue (20% contribution) contours describe regions where negatively charged groups and positively charged groups enhance the activity, respectively. It should be mentioned that this does not mean that the groups in the vicinity of regions not in a colored area have no influence on the activity, because all compounds probably have the same interaction in these areas or due to other reasons.¹⁹

Figure 6 combined steric field information and the impact of putative modification on the biological activity of paclitaxel. For convenience to compare one another, the steric contours were shown in Figure 6 using active compound **12** ((2'*R*,3'*S*)-paclitaxel), less active compound **9** ((2'*S*,3'*R*)-10-acetoxycetaxel), and less active com-

pound **19** ((2'*R*,3'*S*)-2'-acetoxypaclitaxel) as reference molecules, respectively. The steric contours showed that the yellow regions were situated close to the C-2' and C-3' positions of the C-13 side chain, which indicated that additional steric interaction in this region would lead to a decreased activity of the paclitaxel analogue. Previous SAR studies of paclitaxel have revealed that the activity of paclitaxel is crucially dependent on the absolute stereochemistry of the chiral center on C-2' and C-3'. As shown in Figure 6A, C-2' and C-3' in the vicinity of this yellow region were occupied by two hydrogen atoms of (2'*R*,3'*S*)-paclitaxel; small volumes have no influence on the activity. But in the stereoisomers of (2'*R*,3'*S*)-paclitaxel analogues, (2'*S*,3'*R*)-paclitaxel, or (2'*S*,3'*S*)-paclitaxel or (2'*R*,3'*R*)-paclitaxel analogues, fit using paclitaxel as the template molecule as (2'*S*,3'*R*)-10-acetoxycetaxel shown in Figure 6B, the large phenyl ring at C-3' position unfavorably orients toward the yellow region and leads

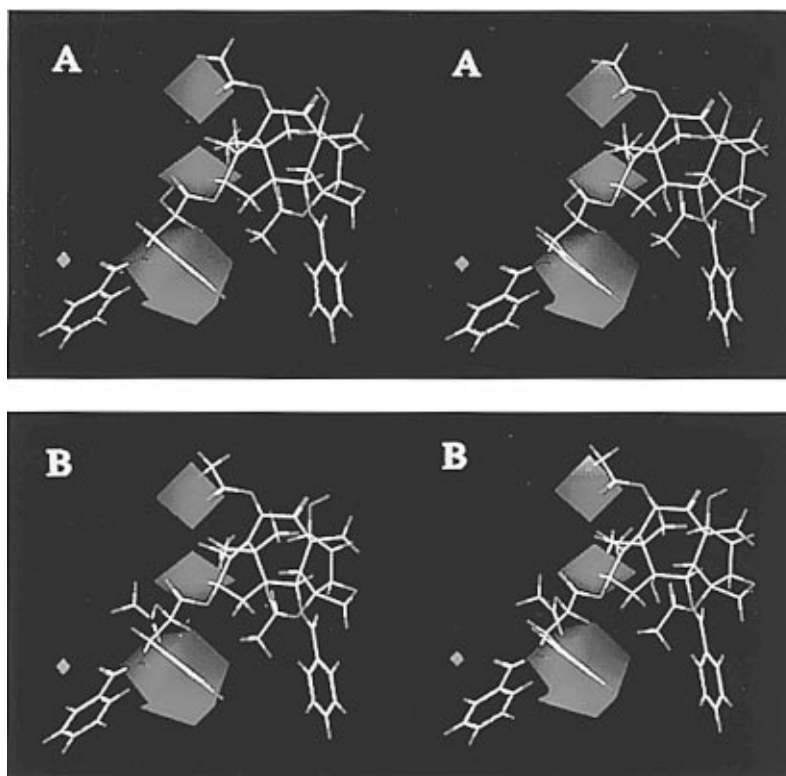


Figure 7. Stereoview of the CoMFA electrostatic sd^*coeff contour plot from the PLS analysis based 80 training set compounds. Positive charge favored areas (contribution level of 80%) are represented by blue polyhedra. Negative charge favored areas (contribution level of 20%) are represented by red polyhedra. Active compound **12** ($(2'R,3'S)$ -paclitaxel) and less active compound **19** ($(2'R,3'S)$ -2'-acetyloxy-paclitaxel) were embedded in A and B, respectively.

to steric hindrance so as to reduce its activity; the other less active stereoisomer is attributed to the same reason. From the orientation of their substituents in 3D space, it is obvious that $(2'R,3'S)$ -paclitaxel analogues have much stronger activity than their stereoisomers. In the tubulin assay, the lower activity of paclitaxel esterified at C-2' OH is partially caused by the large substituents at the C-2' position. Figure 6C intuitively showed that unfavorably bulky acetyl or other large substituents at C-2' close to the yellow region would result in the loss of activity. The other reason will be examined in the following discussion on electrostatic contour maps.

The green region for positive steric contribution mainly occupied two different areas, the phenyl ring at C-3' and phenyl ring at C-3' *N*-acyl (as shown in Figure 6A), and it indicated the importance of bulky substitutions on these two positions for the binding activity. This was demonstrated by greater values of activities of a series of compounds with bulky substituents for C-3' *N*-phenyl, such as *t*BuO, furan, *c*-C₄H₈, and CH₃. In contrast, small groups such as OH, H, and NH₂ always lead to a decrease in biological activity. A similar conclusion can be drawn from the bulky substituents for C-3' phenyl. We noticed that the activity is not significantly affected when one of two phenyl groups was replaced by small groups such as CH₃ (e.g., compound **58** and compound **64**). Hence, the two bulky substituents may commonly exert their action on the activity; while a small group is at one position, the other bulky group is able to compensate for the loss of the smaller group. To investigate their hydrophobicity, we attempted to add hydrophobic parameters to CoMFA analysis, but these were not significant, probably because the hydrophobicities of the stereoisomers cannot

be differentiated from each other. Hansch⁴² and co-workers reported that hydrophobic interaction is very important for colchicine in inhibiting microtubule formation. Although the mechanism of action of taxoid is different from that of colchicine, this result suggests to us that the two phenyl groups of paclitaxel mentioned above may play both a steric and hydrophobic role. Therefore, due to the lack of steric field and hydrophobicity, hydrophilic groups (NH₂, OH) will reduce the activity.

Figure 7 showed the electrostatic contour maps embedded with compound **12** ($(2'R,3'S)$ -paclitaxel) and compound **19** ($(2'R,3'S)$ -2'-acetyloxy-paclitaxel), respectively. The two large blue contours were located near C-2' OH and C-3' NH, respectively, and few red contours were found. The experimental results confirmed that the 2'-OH group plays an important role in the binding of paclitaxel to microtubules, but it remains to be investigated how the 2'-OH exhibits its effect on activity. From the crystal data of docetaxel and some NMR studies of paclitaxel analogues,⁴³ the intramolecular hydrogen bonding between C-1' C=O and C-2' OH as well as between C-2' OH and C-3' NH was found, hence, C-2' OH was considered to be essential for the C-13 side chain of paclitaxel to adopt particular conformation. However, the recent NMR study on the conformation of 2'-acetyloxy-paclitaxel⁴⁴ showed that 2'-acetyloxy-paclitaxel without hydrogen bonding at the C-13 side chain still had the same conformation as paclitaxel in polar solution or crystal state. These findings denied the C-2' OH as an indispensable role for the formation of particular paclitaxel conformation. In Figure 7A, the presence of blue area in the proximity of C-2' OH suggested that positive charge substituents increase the

activity and are in accordance with the steric contour in Figure 6C, which does not allow for the presence of substituents at this position because of the large substituents leading to steric hindrance and the loss of the positive charge contours. C-3' NH surrounded by the other large blue area may have a function similar to that of C-2' OH. From an inspection of these contour maps, it might be deduced that the paclitaxel 2'-OH group, perhaps as a hydrogen bond donor, interacts directly with an amino acid residue of tubulin.

The contour maps mainly distributed in the C-13 side chain. The less extensive yellow area in steric contours (Figure 6) and the blue area in the electrostatic contour (Figure 7) close to C-10 acetyl should have a minor impact on the activity since there are exceptions to this pattern. The effects of the C-2 BzO and C-4 AcO as well as the oxetane ring were not shown in these contour maps; possibly the QSAR model did not include enough compounds modified on these positions or these groups have the same influence on the activity. In the vicinity of C-7 and C-9 positions there are no colored areas, which indicated that modification on these position has less influence on the activity.

Summary and Conclusion

In the absence of knowledge for the three-dimension structure of the ligand-receptor complex, we derived a 3D-QSAR model using a CoMFA methodology for 10 classes of paclitaxel analogues on the basis of the active conformation based on X-ray data and NMR studies on paclitaxel and paclitaxel analogues in polar condition. During investigating the stability of the model, the parameter options only moderately affected cross-validated r^2_{cv} . The higher r^2_{cv} (0.640) indicated that the model had good predictive ability for the compounds studied. This result was further validated by predicting the activities of 14 test compounds. The CoMFA model not only revealed that the groups at the C-13 side chain critically impacted on the activity but also successfully explained the important roles of C-2' OH, phenyl groups at C-3' and C-3' N-acetyl positions, and the stereochemistry of atoms at the C-2' and C-3' positions.

References

- Wani, M. C.; Taylor, H. L.; Wall, M. E.; Coggon, P.; McPhail, A. T. Plant Antitumor Agents VI. The Isolation and Structure of Taxol, a Novel Antileukemic and Antitumor Agent from *Taxus brevifolia*. *J. Am. Chem. Soc.* **1971**, *93*, 2325–2327.
- For review: Rowinsky, E. K.; Donehower, R. C. The Clinical Pharmacology and Use of Antimicrotubule Agents in Cancer Chemotherapeutics. *Pharmacol. Ther.* **1991**, *52*, 35–84.
- For review: Rowinsky, E. K.; Donehower, R. C. Taxol: Twenty Years Later, The Story Unfolds. *J. Natl. Cancer Inst.* **1991**, *83*, 1778–1781.
- For several review on clinical topics, see: Paclitaxel (Taxol) Investigator's Workshop. Proceedings of a Johns Hopkins Oncology Center Workshop. *Semin. Oncol. Suppl.* **1993**, *20*, 1–60.
- Suffness, M. Taxol: From Discovery to Therapeutic Use. In *Annual Reports in Medicinal Chemistry*; Bristol, J. A., Ed.; Academic Press: San Diego, 1993; Vol. 28, Chapter 32, pp 305–314.
- Gueritte-Voegelein, F.; Le Goff, M. T.; Mangatal, L.; Potier, P. Relationship between the Structure of Taxol Analogues and Their Antimitotic Activity. *J. Med. Chem.* **1991**, *34*, 992–998.
- Mangeney, P.; Andriamiamialisoa, Z.; Lallemand, Y.; Laanglois, Y.; Langlois, N.; Potier, P. 5'-NOR Anhydrovinblastine Prototypy of A New Class of Vinblastine Derivatives. *Tetrahedron* **1979**, *35*, 2175–2174.
- Schiff, P. B.; Fant, J.; Horwitz, S. B. Promotion of Microtubule Assembly in vitro by Taxol. *Nature* **1979**, *277*, 665–666.
- Rowinsky, E. K.; Onetto, N.; Canetta, R. M.; Arbus, S. G. Taxol: The First of the Taxanes, and Important New Class of Antitumor Agents. *Seminars Oncol.* **1992**, *19*, 646–662.
- Seidman, A. D. Clinical Results of Taxol in Treatment of Advanced Breast Cancer: Single Agent Trials. Stony Brook Symposium on taxol and taxotere, May 14–15, 1993, Stony Brook, NY, Abstracts pp 14–16.
- Horwitz, S. B. Taxol: Mechanism of Action and resistance. Stony Brook Symposium on Taxol and Taxotere, May 14–15, 1993, Stony Brook, NY, Abstracts pp 23–24.
- Denis, J. S.; Greene, A. E.; Guenard, D.; Gueritte-Voegelein, F.; Mangatal, L.; Potier, P. A Highly Efficient, Practical Approach to Natural Taxol. *J. Am. Chem. Soc.* **1988**, *110*, 5917–5919.
- For review: Georg, G. I.; Ali, S. M.; Zygmunt, J.; Jayasinghe, L. R. Taxol: A Novel Antitumor Agent. *Exp. Opin. Ther. Pat.* **1994**, *4*, 109–120.
- For review: Nicolaou, K. C.; Dai, W.-M.; Guy, R. K. Chemistry and Biology of Taxol. *Angew. Chem., Int. Ed. Engl.* **1994**, *33*, 15–44.
- Taxane Anticancer agents: Basic Science and Current Status*; Georg, G. I., Chen, T. T., Ojima, I., Vyas, D. M., Ed.; American Chemical Society: Washington, DC, 1995.
- Kant, J.; Huuag, S.; Wong, H.; Fairchild, C.; Vyas, D.; Farina, V. Studies toward Structure-Activity Relationships of Taxol: Synthesis and Cytotoxicity of Taxol Analogues with C-2' Modified Phenylisoserine Side Chain. *Bioorg. Med. Chem. Lett.* **1993**, *3*, 2471–2474.
- Swindell, C. S.; Krauss, N. E.; Horwitz, S. B.; Ringgel, L. Biologically Active Taxol Analogues with Deleted A-Ring Side Chain Substituents and Variable C-2' Configurations. *J. Med. Chem.* **1991**, *34*, 1176–1184.
- Kington, D. G. I.; Molinero, A. A.; Rimoldi, J. M. The Taxane Diterpenoids. In *Progress in the Chemistry of Organic Natural Products*; Springer: New York, 1993; pp 1–206.
- Cramer, R. D., III; Patterson, D. E.; Bunce, J. D. Comparative Molecular Field Analysis (CoMFA). 1. Effect of Shape on Binding of Steroids to Carrier Proteins. *J. Am. Chem. Soc.* **1988**, *110*, 5959–5967.
- Lataste, H.; Senilh, V.; Wright, M.; Guenard, D.; Potier, P. Relationships between the Structures of Taxol and Baccatine III Derivatives and Their in vitro Action on the Disassembly of Mammalian Brain and Physarum Amoebal Microtubules. *Proc. Natl. Acad. Sci. U.S.A.* **1984**, *81*, 4090–4094.
- Dubois, J.; Guenard, D.; Gueritte-Voegelein, F.; Guedira, N.; Potier, P.; Gillet, B.; Beloeil, J. C. Conformation of Taxotere and Analogues Determined by NMR Spectroscopy and Molecular Modeling Studies. *Tetrahedron* **1993**, *49*, 6533–6544.
- For review: Hepperle, M.; Georg, G. I. Taxol Analogs. *Drugs Future* **1994**, *19*, 573–584.
- Ali, S. M.; Hoemann, M. Z.; Aube, J.; Georg, G. I.; Mitscher, L. A. Butitaxel Analogue: Synthesis and Structure-Activity Relationships. *J. Med. Chem.* **1997**, *40*, 236–241.
- Ojima, I.; Duclos, O.; Kuduk, S. D.; Sun, C. M.; Slater, J. C.; Lavelle, F.; Veith, J. M.; Bernacki, R. J. Synthesis and Biological Activity of 3'-Alkyl- and 3'-Alkenyl-3'-Dephenyldocetaxels. *Bioorg. Med. Chem. Lett.* **1994**, *4*, 2631–2634.
- Li, I.; Thomas, S. A.; Klein, L. L.; Yeung, C. M.; Maring, C. J.; Grampovnik, D. J.; Lartey, P. A.; Plattner, J. J. Synthesis and Biological Evaluation of C-3'-Modified Analogs of 9(R)-Dihydro-taxol. *J. Med. Chem.* **1994**, *37*, 2655–2663.
- Maring, C. J.; Grampovnik, D. J.; Yeung, C. M.; Klein, L. L.; Li, L.; Thomas, S. A.; Plattner, J. J. C-3'-N-Acyl Analogs of 9(R)-Dihydro-taxol: Synthesis and Structure-Activity Relationships. *Bioorg. Med. Chem. Lett.* **1994**, *4*, 1429–1432.
- Chen, S. H.; Wei, J. W.; Long, B. H.; Fairchild, C. A.; Carboni, J.; Mamber, S. W.; Rose, W. C.; Johnston, K.; Casazza, A. M.; Kadow, J. F.; Farina, V.; Vyas, D. M.; Doyle, T. W. Novel C-4 Paclitaxel (Taxol) Analogs: Potent Antitumor Agents. *Bioorg. Med. Chem. Lett.* **1995**, *5*, 2741–2746.
- Ojima, I.; Duclos, O.; Zucco, M.; Bissery, M. C.; Combeau, C.; Vignard, P.; Riou, J. F.; and Lavelle, F. Synthesis and Structure-Activity Relationships of New Antitumor Taxoids: Effects of Cyclohexyl Substitution at the C-3' and/or C-2' of Taxotere (Docetaxel). *J. Med. Chem.* **1994**, *37*, 2602–2608.
- Boge, T. C.; Himes, R. H.; Vander Velde, D. G.; and Georg, G. I. The Effect of the Aromatic Rings of Taxol on Biological Activity and Solution Conformation: Synthesis and Evaluation of Saturated Taxol and Taxotere. *J. Med. Chem.* **1994**, *37*, 3337–3343.
- Klein, L. L.; Li, L.; Maring, C. J.; Yeung, C. M.; Thomas, S. A.; Grampovnik, D. J.; Plattner, J. J. Antitumor Activity of 9(R)-Dihydro-taxane Analogs. *J. Med. Chem.* **1995**, *38*, 1482–1492.
- Ojima, I.; Fenoglio, I.; Park, Y. H.; Pera, P.; Bernacki, R. J. Synthesis and Biological Activity of 14-Hydroxydocetaxel. *Bioorg. Med. Chem. Lett.* **1994**, *4*, 1571–1576.
- Harriman, G. C. B.; Jalluri, R. K.; Grunewald, G. L.; Vander Velde, D. G.; Georg, G. I. The Chemistry of the Taxane Diterpene: Stereoselective Synthesis of 10-Deacetoxy-11,12-epoxy-paclitaxel. *Tetrahedron Lett.* **1995**, *36*, 8909–8912.
- Chmurny, G. N.; Hilton, B. D.; Brobst, S.; Look, S. A.; Witherup, K. M.; Beutler, J. A. ¹H and ¹³C-NMR Assignments for Taxol, 7-epi-taxol, and Cephalomannine. *J. Nat. Prod.* **1992**, *55*, 414–423. (b) Baker, J. K. Nuclear Overhauser Effect Spectroscopy

- (NOESY) and Dihedral Angle Measurements in the Determination of the Conformation of Taxol in Solution. *Spectrosc. Lett.* **1992**, *25*, 31–48. (c) Falzone, C. J.; Lecomte, J. T. J. Characterization of Taxol in Methylene Chloride by NMR Spectroscopy. *Tetrahedron Lett.* **1992**, *33*, 1169–1172. (d) Hilton, B. D.; Chmurny, G. N.; Musckik, G. M. Taxol: Quantitative Internuclear Proton–Proton Distance in Deuterated Chloroform Solution from NOE Data: 2D NMR ROESY Buildup Rates at 500 Mhz. *J. Nat. Prod.* **1992**, *55*, 1157–1161. (e) Williams, H. J.; Scott, A. I.; Dieden, R. A.; Swindell, C. S.; Chirlan, L. E.; Franel, M. M.; Heerding, J. M.; Krause, N. E. NMR and Molecule Modeling Study of the Conformation of Taxol and of Its Side Chain Methyl Ester in Aqueous and non-Aqueous Solution. *Tetrahedron* **1993**, *49*, 6545–6560. (f) Cachau, R. E.; Gussio, R.; Beutler, J. W. Solution Structure of Taxol Determined Using a Novel Feedback-Scaling Procedure for NOE-Restrained Molecular Dynamics. *Supercomput. Appl. High Perform. Comput.* **1994**, *8*, 24–34. (g) Balasubramanian, S. V.; Straubinger, R. M. Taxol-lipid Intercations: Taxol-Dependent Effects on the Physical Properties of Model Membranes. *Biochemistry* **1994**, *33*, 8941–8947.
- (34) Gueritte-Voegelein, F.; Guenard, D.; Mangatal, L.; Potier, P.; Guilhem, J.; Cesario, M.; Rascard, C. Structure of a Synthetic Taxol Precursor: *N-tert*-butoxycarbonyl-10-deacetyl-*N*-debenzoyl-Taxol. *Acta Crystallogr.* **1990**, *C46*, 781–784. (b) Gao, Q.; Wei, J. M.; Chen, S. H. Crystal Structure of 2-Debenzoyl, 2-Acetoxy Paclitaxel (taxol): Conformation of the Paclitaxel Side-Chain. *Pharm. Res.* **1995**, *12*, 337–341. (c) Gao, Q.; Golik, J. 2'-Carbamate taxol. *Acta Crystallogr.* **1995**, *C51*, 295–298. (d) Mastropaolo, D.; Camerman, A.; Luo, Y.; Brayer, G. D.; Camerman, N. Crystal and Molecular Structure of Paclitaxel (taxol). *Proc. Natl. Acad. Sci. U.S.A.* **1995**, *92*, 6920–6924.
- (35) The program SYBYL 6.0/6.04 is available from Tripos Assoc., 1699 S Hanley Rd, St. Louis, MO 63144.
- (36) Clark, M.; Cramer, R. D., III; Van Opdenbosh, N. Validation of the General purpose Tripos 5.2 Force Field. *J. Comput. Chem.* **1989**, *10*, 982–1012.
- (37) Powell, M. J. D. Restart Procedure for the Conjugate Gradient Method. *Math. Program* **1977**, *12*, 214.
- (38) Wold, S.; Albano, C.; Dunn, W. J., III; Edlund, U.; Esbensen, K.; Geladi, P.; Hellberg, S.; Johansson, E.; Lindberg, W.; Sjostrom, M. Multivariate Data Analysis in Chemistry. In *CHEMOMETRICS: Mathematics and Statistics in Chemistry*; Kowalski, B., Ed.; Reidel: Dordrecht, The Netherlands, 1984. (b) Sybyl Molecular Modeling Software, version 6.02, 1993. Tripos Associates, Inc., St. Louis, MO 63144; Sybyl theory manual, 1993.
- (39) Cramer, R. D., III; Bunce, J. D.; Patterson, D. E.; Frank, I. E. Crossvalidation, Bootstrapping, and Partial Least Squares Compared with Multiple Regression in Conventional QSAR Studies. *Quant. Struct.-Act. Relat.* **1988**, *7*, 18–25.
- (40) Klebe, G.; Abraham, U. On the Prediction of Binding Properties of Drug Molecules by Comparative Molecular Field Analysis. *J. Med. Chem.* **1993**, *36*, 70.
- (41) Oprea, T. I.; Garcia, A. E. Three-Dimensional Quantitative Structure–Activity Relationships of Steroid Aromatase Inhibitors. *J. Comput.-Aided Mol. Des.* **1996**, *10*, 186–200.
- (42) Hansch, C.; Telzer, B. R. and Zhang, L. T. Comparative QSAR in Toxicology: Examples from Teratology and Cancer Chemotherapy of Aniline Mustards. *Crit. Rev. Toxicol.* **1995**, *25*, 67–89.
- (43) Guenard, D.; Gueritte-Voegelein, F.; Potier, P. Taxol and Taxotere: Discovery, Chemistry, and Structure–Activity Relationships. *Acc. Chem. Res.* **1993**, *26*, 160–167.
- (44) Williams, H. J.; Moyna, G.; Scott, A. I. NMR and Molecular Modeling Study of the Conformation of Taxol 2'-Acetate in Chloroform and Dimethyl Sulfoxide Solutions. *J. Med. Chem.* **1996**, *39*, 1555–1559.

JM970442U